Three-dimensional finite element analysis: Anatomical splint fixation for Colles fractures

FEI HUANG[1], RUI TAN[1], MENG-WEI WANG[1], LIU-CHAO HU[1], ZHI WANG[2], SHI-DONG SUN[1], JIE-WEN HUANG[1] and YI-WEN LUO[1]

Departments of [1]Traumatology and [2]Operating Room, The Third Affiliated Hospital of Guangzhou University of Chinese Medicine, Guangzhou, Guangdong 510000, P.R. China

Received June 20, 2023; Accepted December 21, 2023

DOI: 10.3892/etm.2024.12386

Abstract. With the rapid development of digital research in clinical orthopedics, the efficacy and safety of splint fixation can be better evaluated through biomechanical analysis based on a three-dimensional (3D) finite element model. It is essential to address the current gap in understanding the biomechanical implications of anatomical splint fixation for Colles fractures. By employing advanced 3D finite element analysis, the present study aimed to provide a comprehensive evaluation, offering valuable insights that can contribute to enhancing the effectiveness of anatomical splint fixation in the clinical management of Colles fractures. The 3D finite element models of the forearm and hand were constructed using Mimics 15.0 according to data from computed tomography of a patient with a Colles fracture. After the validity of the model was verified, the corresponding material properties of the models were adjusted to simulate a Colles fracture. Subsequently, the reduction functions, such as radial inclination and ulnar deviation, of the simulated fracture were completed and the mechanical changes of the tissues surrounding the fracture were calculated. Anatomical splints were then placed on the surfaces of the 3D finite element models of Colles fractures at various positions to analyze the changes in the stress cloud diagram, such as for the soft tissue and anatomical splints. In the present study, the constructed 3D finite element models were accurate and valid. The maximum stress of the anatomical splints and soft tissues was 2.346 and 0.106 MPa in pronation, 1.780 and 0.069 MPa in median rotation and 3.045 and 0.057 MPa in supination, respectively. Splint stress reached the highest level in supination and soft tissue stress achieved the highest level in pronation. The peak of splint stress occurred during supination, which contrasts to the peak of soft tissue stress observed in pronation, suggesting splint fixation median rotation can effectively avoid compression of the local soft tissue.

Correspondence to: Dr Yi-Wen Luo, Department of Traumatology, The Third Affiliated Hospital of Guangzhou University of Chinese Medicine, 261 Longxi Avenue, Liwan, Guangzhou, Guangdong 510000, P.R. China
E-mail: gzzyydxlyw@126.com

Key words: Colles fracture, anatomical splint, finite element analysis, median rotation

Introduction

Colles fractures, which are usually caused by low-energy injuries, refer to fractures that occur within 3 cm of the articular surface of the distal radius. As one of the most commonly occurring fractures, Colles fractures account for 90% of distal radius fractures (1). They are characterized by the displacement of the distal radius and dorsal, as well as the proximal volar displacement (2). There are several causes of a Colles fracture; the most common is a metacarpus landing after an accidental fall and most occur in elderly individuals aged >60 years (3). At present, most treatments for Colles fractures are conservative and include manual reduction followed by splint fixation, which can achieve satisfactory results for simple and stable extra-articular fractures and some intra-articular fractures (1). Anatomical splints are an effective method for the fixation and healing of Colles fractures (4).

In recent years, computational biomechanics analysis technology has gradually been integrated into the clinical application and basic research of medicine. Notably, finite element analysis (FEA) is the most widely applied tool in the field of orthopedics (5). FEA was first proposed by Professor Clough in 1960 as an effective method to calculate the discrete value (6) and analyze the structural stress and deformation. Specifically, FEA can reduce complex problems into simple ones, thereby solving complex clinical or experimental problems using simple methods (7). In 1972, Rybicki *et al* (8) and Brekelmans *et al* (9) applied FEA in the field of orthopedic biomechanics research. Currently, advances in computer technology have facilitated the rapid development of FEA. Specifically, FEA modeling has developed from the two-dimensional (2D) to the three-dimensional (3D) and the material properties have progressed from linear to nonlinear. In addition, the methods to construct the finite element mesh models have evolved from simplified modeling by computer alone to the introduction of computed tomography (CT) or magnetic resonance imaging (MRI).

With the increasing development of digital research in clinical orthopedics, FEA has been applied in plastic surgery, spinal

limbs, articular cartilage and bone microstructure research. In addition, FEA has also played a role in high-simulation data models associated with ligament muscles, joint capsules and other soft tissues (10). 3D finite element analysis, with its inherent advantages for biomechanical research (11), surpasses the limitations of traditional experiments and is gradually being used in the research of knee joint problems. The efficacy and safety of splint fixation can be better evaluated through biomechanical analysis based on a 3D finite element model. Therefore, the present study explored the biomechanical distribution in various positions with stable efficiency to maintain the Colles fractures for anatomical splint fixation through the establishment of a 3D finite element model of Colles fractures.

Materials and methods

Ethics statement. The present study was conducted in accordance with the Declaration of Helsinki (as revised in 2013). It was approved by ethics the committee of The Third Affiliated Hospital of Guangzhou University of Chinese Medicine and oral informed consent was obtained from the patient.

Materials. The Toshiba CT machine was obtained from Canon Medical Systems Corporation. The bones were defined as having isotropic homogeneous elastic material properties, ligaments served as the shell elements and the various components are presented in Table I. Mimics 15.0 software (Materialise NV) was used to construct the 3D models. ANSYS Workbench software (ANSYS Inc.) was used to create the 3D finite element model. Imageware 5.0 (Siemens AG) was used for smoothing, denoising, paving and other modifications to refine and optimize the model.

Establishment of a 3D finite element model of the forearm. Clinical CT data was obtained from a patient with a Colles fracture [male; aged 34 years; Arbeitsgemeinschaftfür Osteosynthesefragen (AO) classification (12) of fracture: A2] and without other soft tissue or bone disorders. In addition to the fracture end, the anatomy of the patient, except for the fractured region, was anatomically consistent with the uninjured side. To acquire detailed anatomical information, a 64-slice spiral CT scanning procedure was performed using the Toshiba CT machine. The patient assumed a supine position with spontaneously drooping arms during the scan. The scanning range included the proximal forearm to the distal finger, with the parameters set at a slice thickness of 0.6 mm with a total of 1,000 slices. Subsequently, the obtained CT data were saved in DICOM3.0 format (13).

The collected data were then processed using Mimics 15.0 software (Materialise NV) to construct the 3D models (Fig. 1). The segmentation and reconstruction of the bone structure in the image and the adjustment of the connection between the joints, such as between the radius and wrist, were performed so that they were in a fusion state. At the same time, digital models of soft tissues in the different parts were established using the aforementioned methods. The bone structure and soft tissue model were imported into Imageware 5.0 (Siemens AG) for smoothing, denoising, paving and other modifications to refine and optimize the model. The optimized model was inputted into PRO/E software (version 5.0; Parametric Technology Corporation) for assembly. Based on the anatomical locations described in the literature (14-16), the appropriate components were selected from the parts library of the software and structures such as ligaments, cartilage and fibrocartilage were added to obtain a 3D model of the forearm and hand. This model was inputted into ANSYS Workbench software (ANSYS Inc.) to construct the 3D finite element model of the forearm and hand (Fig. 2).

Table I. Tissue parameters of various parts of the human body.

Material	Elastic modulus	Poisson's ratio
Compact bone	13.3 GPa	0.30
Cancellous bone	0.69 GPa	0.30
Cartilage	10 MPa	0.45
Ligament	0.3 GPa	0.40
Interosseous membrane	0.95 GPa	0.45
Soft tissue	0.15 MPa	0.49
Fracture line	50 kPa	0.05

Data from Wang Yijin and Wang Jielin, *Orthopaedic Biomechanics*, First Edition, Beijing: People's Army Medical Press, 1986.

Validation of the 3D finite element model. Contact relationships within the model were established in accordance with current literature. Specifically, the bone-to-bone and interior of the bones were designated as 'Contact', while bone-to-soft tissue interactions were defined as 'Tie'. The friction coefficient within joints was intentionally disregarded. To simulate realistic conditions, the radius and proximal ulna were constrained using full degree of freedom fixation. Subsequently, a 100 N axial compression load was applied to the second and third metacarpals, according to established protocols (17-22). To validate the model, it was subjected to loading in different directions to ensure that the generated stress patterns were consistent with the expected biomechanical responses. The material properties of the model were fine-tuned to simulate the conditions of a Colles fracture. Reduction functions and mechanical changes around the simulated fracture site were incorporated into the model to enhance realistic conditions. This validation approach ensured the fidelity of the 3D finite element model and its suitability for biomechanical analysis and it adhered to the established methodologies in the field.

Finite element analysis

Load configuration and boundary constraint. The degrees of freedom of all nodes (displacement and rotation in three directions) for the upper radioulnar notch of the proximal section of the 3D finite element model were defined as 0. For the loading under a dynamic state, the compressive force of the body was assumed to occur from the proximal to the distal forearm; the vertical upward component was received by the surface of the wrist, radius and ulna joints was set as 100 N; and the tensile component as 100 N. When simulating the internal rotation of the forearm, the stress on the radius arose from the internal rotation; the loaded torsional moment was 1 Nm; and vertical moments were applied to the medial and lateral distal radius

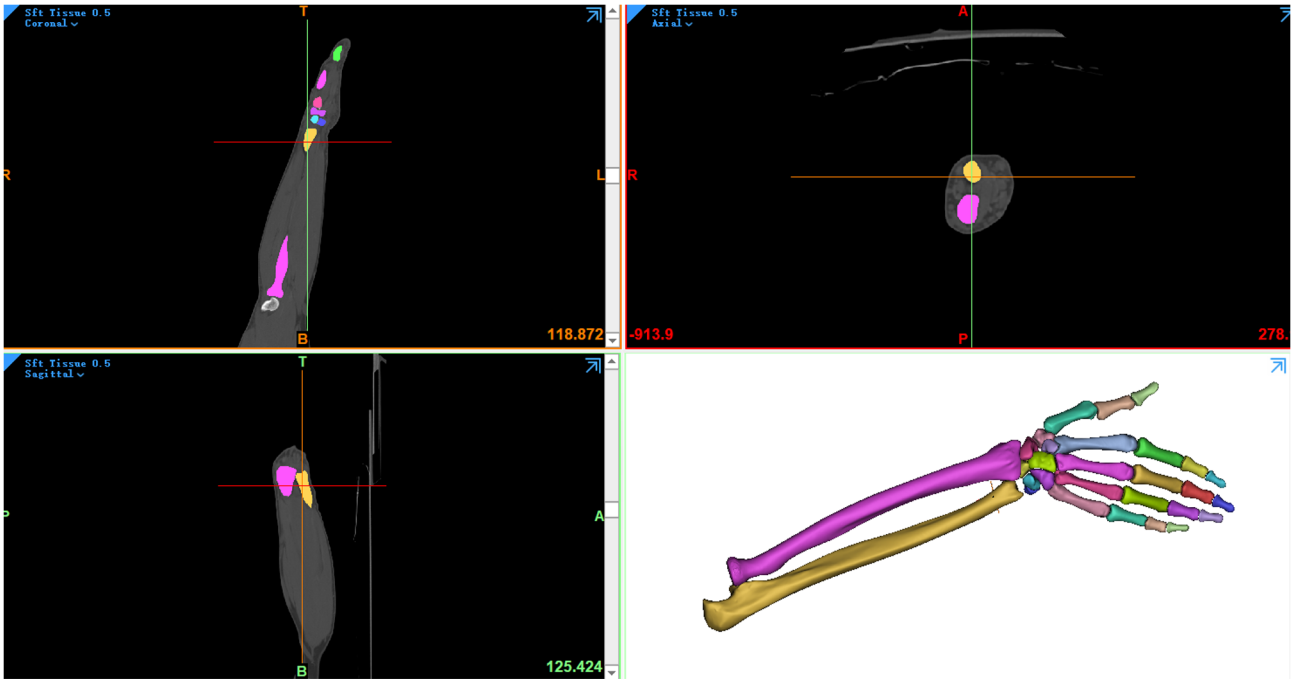

Figure 1. Construction of 3D models. 3D, three-dimensional.

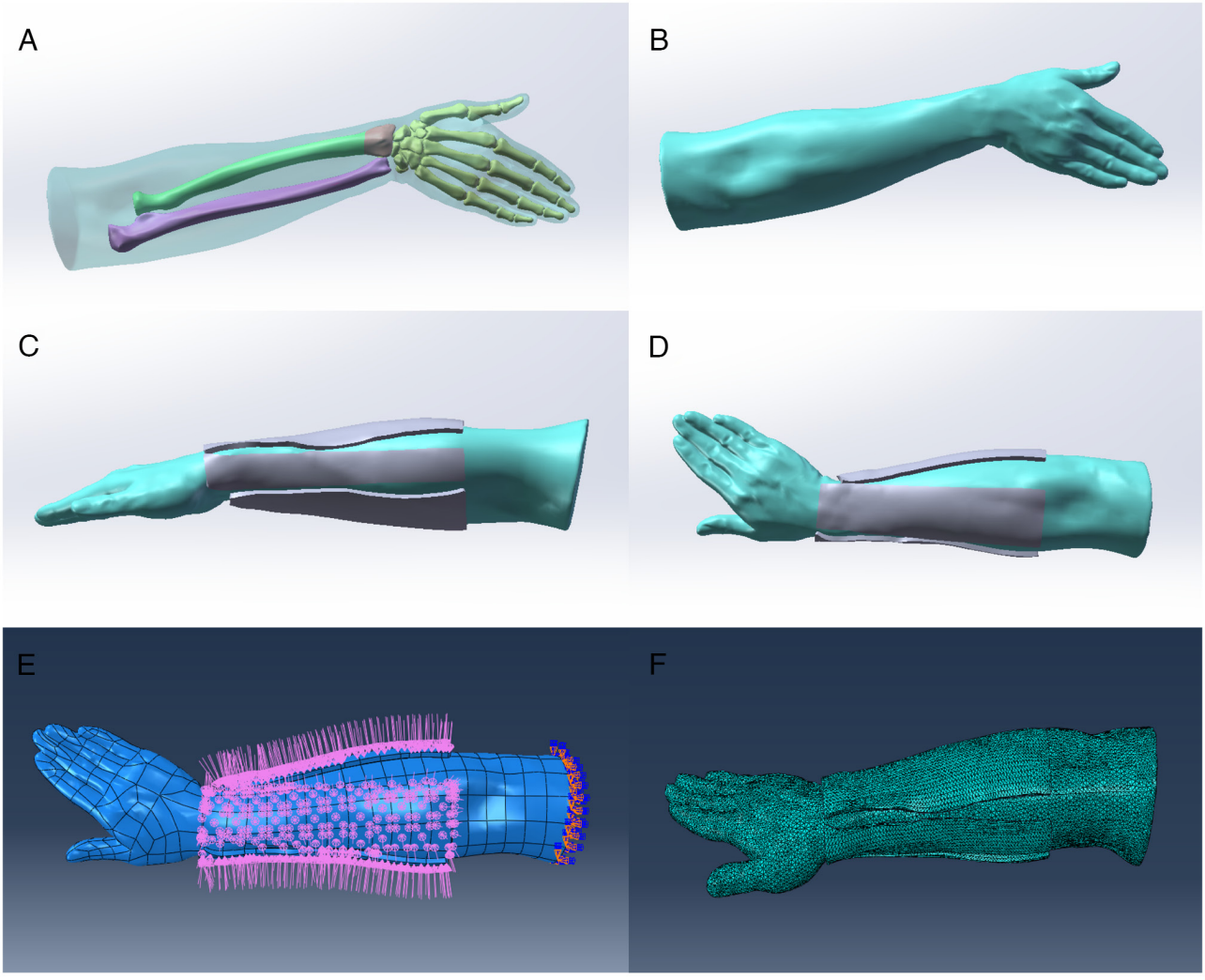

Figure 2. Construction of 3D finite element model of Colles fracture. (A) 3D model of forearm bones; (B) 3D model of forearm skin; (C and D) 3D model of fixation with small splints; (E) Loads configuration and boundary constraints; and (F) Mesh convergence. 3D, three-dimensional.

to simulate the working condition of the distal radius under torsional stress.

The boundary constraints for the finite element model of a Colles fracture are the restrictions on the radius and ulna. The full degree of freedom fixation method was applied to constrain the radius and ulna, thus simulating their basic positions to keep them relatively stationary in the model. For the conditions for the ligaments and soft tissues, the material properties and geometric shapes of the ligaments and soft tissues were considered to simulate their behavior under physiological conditions. This involved treating the ligaments as shell elements and assigning appropriate properties based on previously reported data (Table I).

Mesh convergence. Mesh convergence was performed for all the obtained bone structure and soft tissue model using 3-matic (v5.1, Materialise company, Belgium). To generate the finite element model of the volume meshes, the models were imported into ANSYS.13.0 (ANSYS Inc.) and meshed using the SOLID72 element type. SOLID72 is an element that is defined by four nodes, each of which has six degrees of freedom: displacement in the axis x, y and z directions, as well as rotation around the axis x, y and z directions. The finite element mesh model is shown in Fig. 2F.

Simulation and calculation of anatomical splint fixation state. The models were inputted into the ANSYS Workbench software (ANSYS Inc.) and through the automatic block function of the software, higher-order tetrahedron models were selected for the model segmentation. In the segmented model, fixation constraints for the full degrees of freedom for the proximal radius and ulna were determined. A load of 28 N was applied uniformly to each splint, the surface perpendicular to the splint was considered the center and the calculation started from the moment of contact with the skin and ended when mechanical stability was achieved between the splint and skin (23). Under a 28 N load, the body surface stress cloud diagrams and peak values of the anatomical splints in the three different positions (pronation, median rotation and supination) were measured. The measurement indicators mainly included stress distributions in the different parts (e.g., tendons, ulnar head and thenar muscles) as well as the bone surface stress diagrams and peaks. As for the simulation for lateral rotation, the stress on the radius was from lateral rotation; the loaded torsional moment was defined as 1 Nm; and vertical moments were imposed on the medial and lateral distal radius to simulate the working conditions of the distal radius under torsional stress. Finally, the aforementioned boundary conditions and loading were imported into the ANSYS Workbench software (ANSYS, Inc.) and the stress distribution was then analyzed via a 3D finite element model.

Statistical analysis. By using computational tools such as Mimics 15.0 (Materialise NV), Imageware 5.0 (Siemens AG), PRO/E (Parametric Technology Corporation) and ANSYS Workbench (ANSYS Inc.), the present study ensured the accuracy and validity of the 3D models. The loaded 3D finite element model was then assessed in various directions and its validity was confirmed through stress analysis. Data of stress and displacement were expressed as the mean ± standard deviation. Student's t test (unpaired) was used to compare stress and displacement between the anatomical splints and soft tissue. All tests were two-tailed and $P<0.05$ was considered to indicate a statistically significant difference. All statistical analyses were performed using SPSS 26.0 (IBM Corp.).

Results

Verification of the forearm model. The radiocarpal tissue stress was calculated according to the present finite element model. The results of the present study indicated that the stress distribution of the radiocarpal tissue was not uniform; the maximum stress was located in the scaphoid and lunate fossae of the articular surface of the distal radius. Furthermore, the maximum contact stress at the wrist joint surface was 9.57 MPa. According to a previous report (4), the maximum contact stress was ~9 MPa and the stress was mainly distributed in the scaphoid and lunate fossae of the joint surface of the distal radius, which is consistent with the results of this study. Similar simulation results were reported in other literature (24,25). Therefore, the forearm model was determined to be accurate and effective.

Distribution of soft tissue stress and displacement in different body positions

Soft tissue stress distribution in pronation. The stress distribution was consistently uniform across the various radial fracture positions and encompassed critical anatomical structures such as the thenar muscles, radial styloid process and ulnar head. During pronation, the absolute stress of anatomical splints was 0.491±0.346 MPa, reaching a maximum of 2.346 MPa, whereas soft tissues exhibited significantly lower values with 0.012±0.006 MPa and a maximum of 0.106 MPa ($P<0.001$; Table II). In addition, the anatomical splints and soft tissue exhibited the similar absolute displacement (4.676±1.220 vs. 4.210±1.531, $P>0.05$), but the soft tissues had bigger displacement in x-axis than the anatomical splints (-2.450±1.462 vs. -3.490±2.929; $P=0.007$; Table II). The distribution pattern of the anatomical splints and soft tissue stress during the pronation position is visually presented in Fig. 3, which provides detailed insight into the biomechanical response in this specific configuration.

Soft tissue stress distribution in median rotation. In Fig. 4, the stress distribution within the radial fracture displayed a relatively dispersed pattern, with a notable concentration observed in the dorsal wrist, hypothenar, radial styloid process and other relevant anatomical regions. During median rotation, the absolute stress of anatomical splints was 0.409±0.211 MPa, reaching a maximum of 1.780 MPa, whereas soft tissues exhibited significantly lower values with 0.012±0.007 MPa and a maximum of 0.069 MPa ($P<0.001$; Table II). in addition, the anatomical splints and soft tissue exhibited a similar absolute displacement (8.117±2.542 vs. 7.908±3.143; $P>0.05$), but the soft tissues had bigger displacement in z-axis compared with the anatomical splints (-1.883±0.943 vs. -2.329±0.986, $P=0.023$; Table II).

Soft tissue stress distribution in supination. The stress distribution within a radial fracture exhibited a systematic pattern, with the stress concentration notably centered around the key anatomical landmarks, including the wrist joint, radial styloid process, ulnar head and thenar region. During supination, the absolute stress of anatomical splints was 0.562±0.456

Table II. Distribution of anatomical splints and soft tissue stress and displacement in different body positions.

	Pronation				Median rotation				Supination			
Variables	Anatomical splints	Soft tissues	*t*-value	P-value	Anatomical splints	Soft tissues	*t*-value	P-value	Anatomical splints	Soft tissues	*t*-value	P-value
Stress (x-axis)	-0.0003±0.145	-0.020±0.026	0.93	0.354	-0.006±0.077	-0.014±0.022	1.766	0.081	-0.009±0.144	-0.026±0.026	0.822	0.413
Stress (y-axis)	-0.006±0.041	-0.025±0.028	2.684	0.009	0.007±0.117	-0.013±0.021	1.190	0.237	-0.013±0.066	-0.029±0.026	1.595	0.114
Stress (z-axis)	0.076±0.517	-0.022±0.025	1.335	0.185	0.076±0.322	-0.013±0.021	1.950	0.054	0.020±0.699	-0.027±0.024	0.475	0.636
Stress (absolute)	0.491±0.346	0.012±0.006	9.707	<0.001	0.409±0.211	0.012±0.007	13.30	<0.001	0.562±0.456	0.013±0.007	8.512	<0.001
Displacement (x-axis)	-3.490±2.929	-2.450±1.462	-2.226	0.007	1.234±1.153	0.855±0.868	1.857	0.066	-2.151±0.627	-2.162±0.815	0.076	0.940
Displacement (y-axis)	-2.456±1.632	-2.567±1.388	0.361	0.719	-7.464±2.719	-7.452±3.311	0.020	0.984	-3.189±0.878	-3.250±0.893	0.344	0.731
Displacement (z-axis)	-1.874±0.487	-1.677±0.778	-1.505	0.136	-2.329±0.986	-1.883±0.943	2.312	0.023	-2.356±0.225	-2.154±0.602	2.223	0.029
Displacement (absolute)	4.676±1.220	4.210±1.531	1.667	0.099	8.117±2.542	7.908±3.143	0.366	0.716	4.595±0.672	4.532±1.078	0.351	0.727

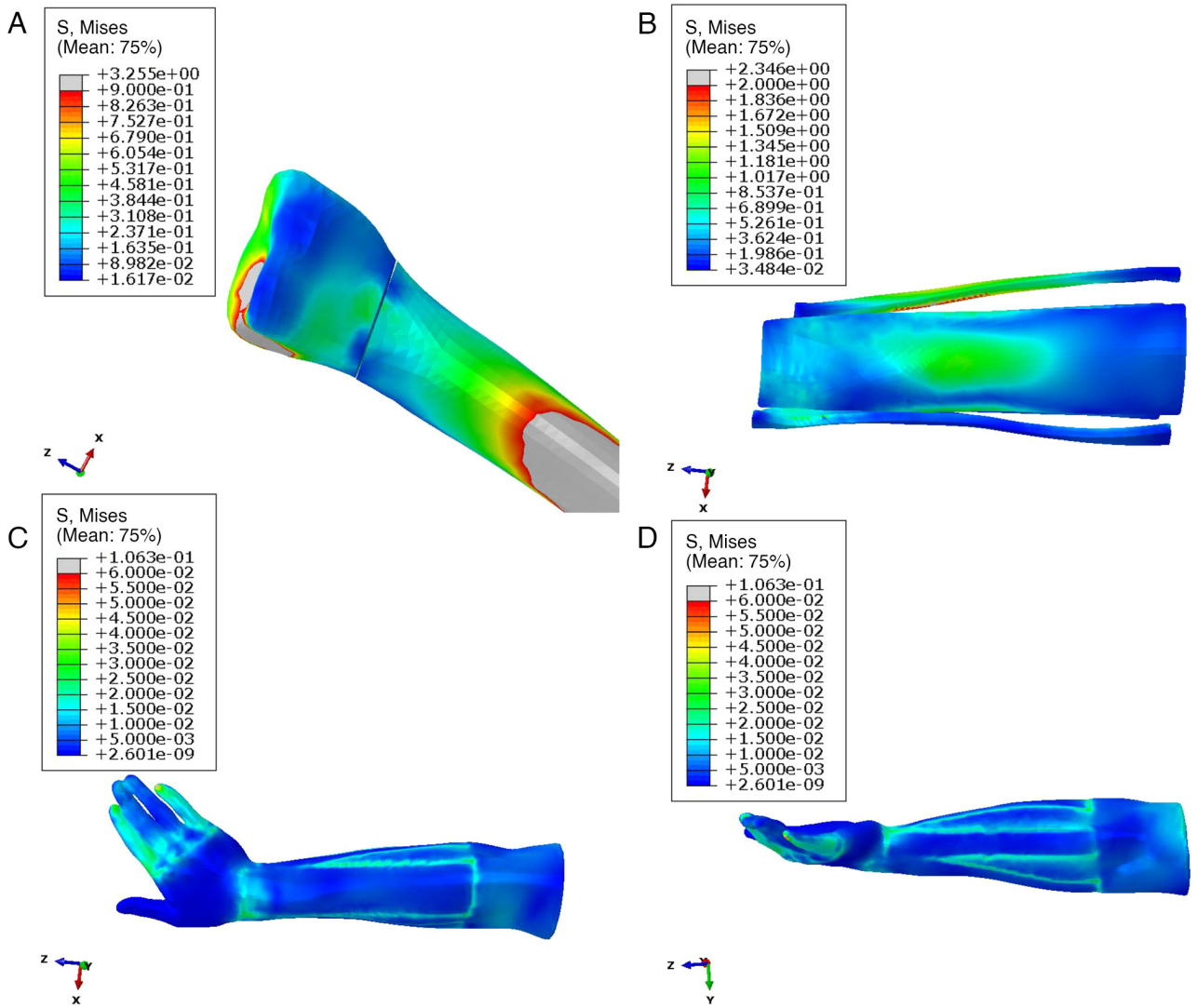

Figure 3. Distribution of soft tissue stress in pronation. (A) Soft tissue and (B) anatomical splint stress distributions; (C) palmar and (D) dorsal palmar.

MPa, reaching a maximum of 3.045 MPa, whereas soft tissues exhibited significantly lower values with 0.013±0.007 MPa and a maximum of 0.057 MPa (P<0.001; Table II). In addition, the anatomical splints and soft tissue exhibited a similar absolute displacement (4.595±0.672 vs. 4.532±1.078, P>0.05), but soft tissues had bigger displacement in z-axis than the anatomical splints (-2.154±0.602 vs. -2.356±0.225, P=0.029; Table II). A comprehensive visualization of this stress distribution and intensity is presented in Fig. 5, offering a detailed depiction of the biomechanical response in the context of radial fracture conditions.

Discussion

Biomechanical research is usually not widely conducted because of technical and ethical restrictions. The tissue attributes of human specimens are unstable and the replication of their physiological environment is challenging; however, biomechanical research relies almost exclusively on the instrumental testing, thus incurring extremely high costs (26). Biomechanical FEA is generally performed via a 3D model that is similar to the human body. Specifically, the 3D model is constructed based on, for example imaging data, material properties, loads, and boundary conditions and the local regional information can be acquired after the simulation of the structure, parameters and loads of the 3D model (4). In general, biomechanical FEA is distinguished by its cost-effectiveness, swift calculation cycle, high simulation accuracy and excellent reproducibility. In recent years, FEA has been increasingly applied to bone and joint stress analysis, fracture risk prediction, internal fixator design and surgical treatment guidance. A previous study established a 3D finite element model of Colles fractures for the first time, thus providing a reference for clinical work (27).

Colles fractures are a relatively common disorder that are mainly caused by indirect violence and can result in joint deformity, limited mobility, pain and swelling and are usually treated conservatively (28,29). Presently, the outcomes of fixation differ based on the materials employed in clinical practice. Compared with traditional fixation with a gypsum plate, fixation with small splints is more flexible and conducive to blood reflux, movement and distraction of soft tissues around the fracture (30). Under actual physiological conditions, tissues such as bone, cartilage, ligaments and interosseous

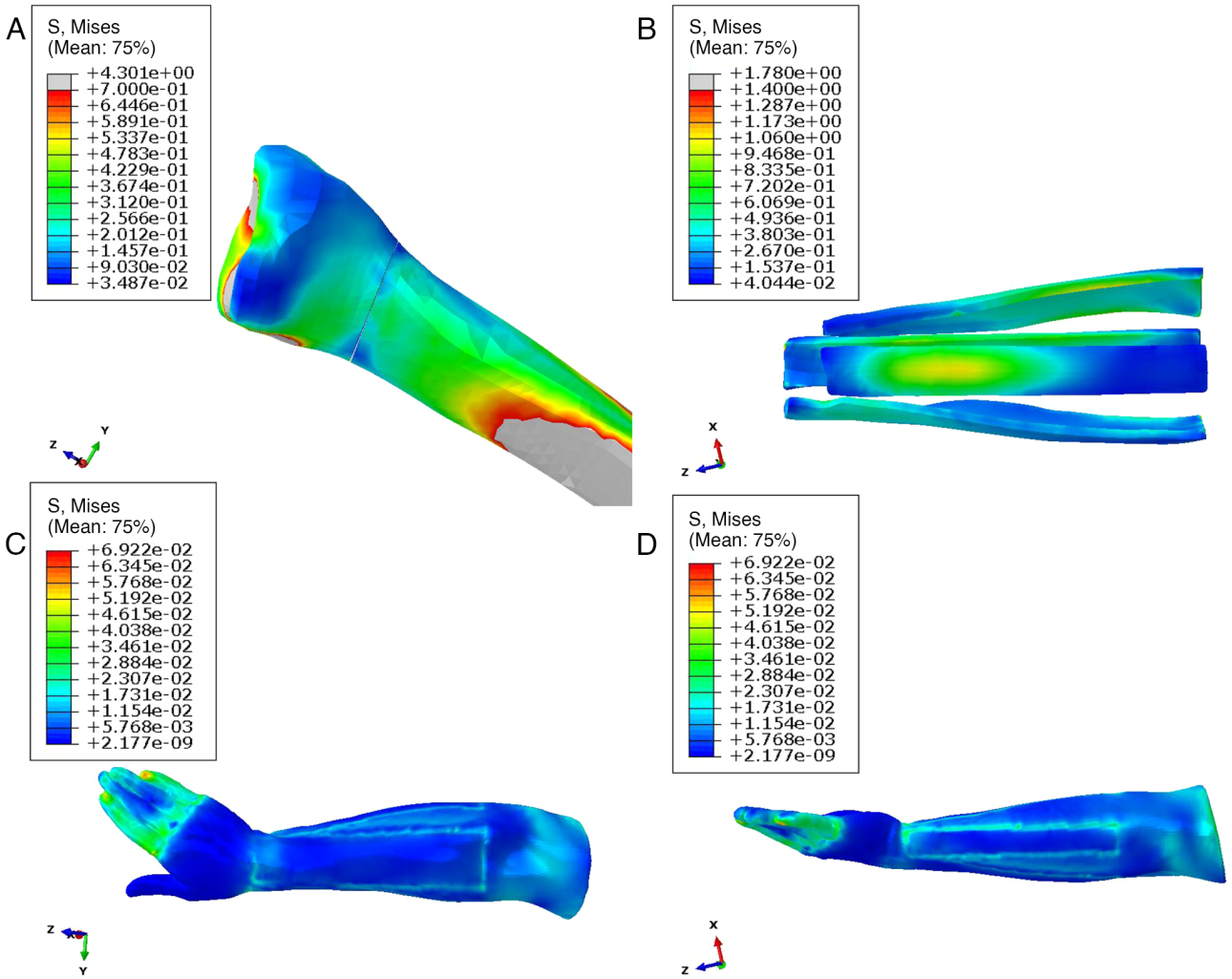

Figure 4. Stress distribution of soft tissue in median rotation. (A) Soft tissue and (B) anatomical splint stress distributions; (C) palmar and (D) dorsal palmar.

membranes do not fully exhibit elastic, linear and isotropic behavior. This is because biomaterials may exhibit complex nonlinear responses under external effects, which are influenced by various factors, including deformation rate, loading history and humidity (31). In the present finite element model, elastic, linear and isotropic properties were chosen mainly to simplify the model, to improve computational efficiency and make it easier to interpret. However, in biomechanical research, understanding the true performance of biological tissues is crucial. In reality, materials such as bones, cartilage and ligaments may exhibit nonlinear, time-varying, or anisotropic behavior under different load conditions. This may be influenced by the complex structure and diversity of biological tissues, as well as their interactions with the surrounding environment (32). To simulate these nonlinear behaviors more accurately, it is necessary to use more complex material models, such as hyperelastic models and progressive failure models, for an improved reflection of the true performance of biomaterials (33). However, such a model can also increase computational complexity and resource requirements. The present study made compromises in model selection to ensure a preliminary simulation of the fracture situation, but it was also realized that this is a simplification that requires further exploration in actual biomechanical research.

There are a few reports on FEA for fractures fixed by splints. Hua *et al* (4) explored the biomechanics of splint fixation of distal radius fractures using three different materials by 3D FEA and analyzed the cloud diagrams of the stress distribution in the soft tissue and bone joints from the forearm to the wrist joint. CT scans were used to obtain the models in that study. As the constitutive equation of various tissues of the human body cannot be provided through relevant mechanical experiments or basic research, the heterogeneity and anisotropy of the tissue material of the human body were assumed to be homogeneous and isotropic linear elastic materials in the present study. According to the model and calculation results, the stress distribution of the limb soft tissue was uniform and the stress of easy entrapment sites such as the apophysis and thenar region was small. Furthermore, maximum stress of the anatomical splints and soft tissues was 2.346 and 0.106 MPa in pronation, 1.780 and 0.069 MPa in median rotation and 3.045 and 0.057 MPa in supination, respectively. Therefore, the stress on the median rotation was minimal, providing a reliable biomechanical basis for the clinical application of anatomical splints. A notable departure is the examination of positions such as pronation, median rotation and supination, shedding light on diverse stress patterns. However, as in Hua *et al* (4), the present study assumed the tissue material of the human

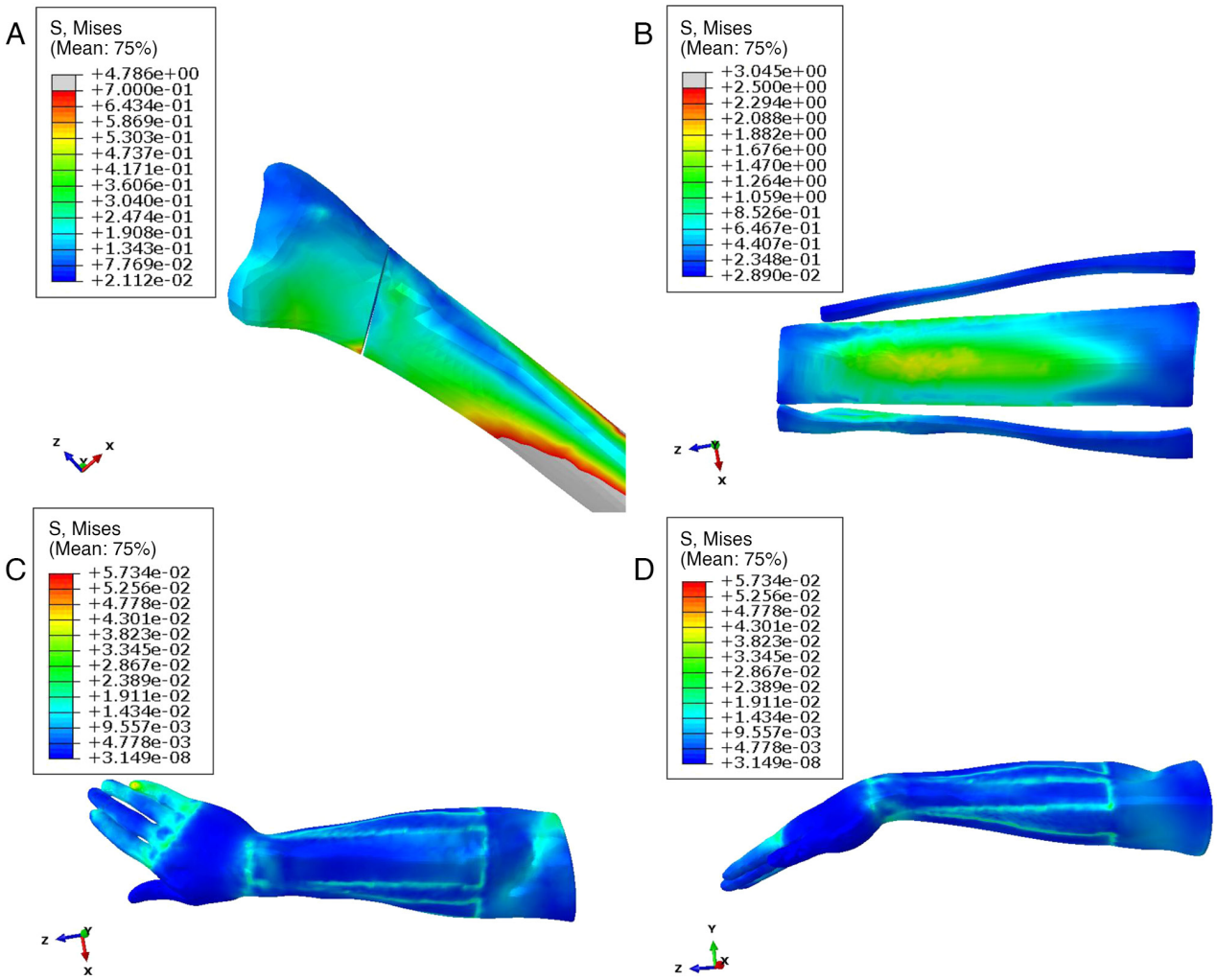

Figure 5. Stress distribution in radial fractures. (A) Soft tissue and (B) anatomical splint stress distributions; (C) palmar and (D) dorsal palmar.

body to be homogeneous and isotropic linear elastic materials due to the unavailability of constitutive equations through relevant mechanical experiments or basic research. In contrast to the emphasis on distal radius fractures in Hua *et al* (4), the present study focused on Colles fractures, revealing distinct stress distribution characteristics in anatomical splints and soft tissues across different positions.

According to the FEA results, it can be observed that the stress at the fracture site is minimal in the neutral position, indicating the highest stability of the fracture. This conclusion is drawn based on experimental findings. The forearm is composed of two bones, the ulna and radius, along with the interosseous membrane between them. The interosseous membrane is a dense connective tissue that not only serves to connect and transmit forces between the two bones but also provides stability, thus limiting the maximum rotational movement of the forearm. Previous research, including anatomical studies, suggests that the interosseous membrane is most relaxed in the neutral position, where it exerts the least traction on the bones and contributes to the overall stability of the fracture site (34-36). Additionally, using a splint for external fixation after a fracture, with the forearm fixed in the neutral position, promotes functional recovery (37). This approach is advantageous because fixing the forearm in pronation or supination positions is less stable than fixing it in the neutral position. In addition, after removing the splint, restoring the supination position is more challenging than restoring the neutral position if it was initially fixed in pronation and vice versa. The 3D FEA of the biomechanics revealed that anatomical splints maintained the palmar tilt and ulnar deviation fixation in Colles fractures. As a rotating limb, different positions of the forearm could cause changes to the mechanical structure (38). Additionally, the stress analysis of Colles fractures fixed with anatomical splints indicated that the maximum soft tissue stress was in pronation and the maximum splint stress was in supination. Taken together, the application of anatomical splints to fix the limb in neutral position can effectively avoid local soft tissue compression and facilitate the healing of the fracture.

In the present study, a finite element model of Colles fractures was precisely designed, considering the various contact interactions crucial to simulate the realistic biomechanical responses. The model incorporated distinct contact types: 'Bone-to-Bone Contact' for interactions between different bone structures such as the radius and ulna; 'Interior of Bones' to represent the internal bone interactions; and 'Bone-to-Soft Tissue Contact' which specified connections between the bones and soft tissues, such as ligaments. The decision to set the friction coefficient within

the joints as negligible aimed to simplify the model while focusing on the primary factors influencing the stability and stress distribution in Colles fractures. This approach aligns with the established biomechanical models, which ensures a comprehensive understanding of the intricate interactions within the finite element model and enhances the reliability of the simulation results.

However, there were still some limitations. The finite element model used in this study was relatively simple. In addition, the model in this study neglects the intrinsic influence of dynamic structures such as muscles and tendons and is unable to simulate the stress of various materials in functional training. In addition, FEA also has some limitations. For instance, the finite element model can only approach the real situation but cannot fully replicate the actual environment. Therefore, the authenticity and validity of the above results need to be verified through additional experiments. Further study can be focus on conducting a long-term follow-up study is imperative to assess the sustained efficacy and potential complications associated with anatomical splint fixation for Colles fractures. This longitudinal investigation will provide crucial insights into the enduring effectiveness of the treatment and its impact on key clinical indicators. Furthermore, comparative studies should be undertaken to juxtapose anatomical splint fixation with alternative treatment modalities such as traditional fixation methods or surgical interventions. Through a comprehensive comparison of the biomechanical effects and clinical outcomes of different therapeutic approaches, a clearer understanding of the advantages and disadvantages of anatomical splint fixation can be elucidated. In addition, patient stratification studies are essential to evaluate the effects of anatomical splint fixation across diverse patient subgroups, considering varying characteristics of Colles fractures or pertinent medical histories. This stratified approach will facilitate the assessment of treatment efficacy in different patient cohorts, thereby contributing to personalized treatment strategies and the optimization of therapeutic interventions.

The present study revealed that the apex of splint stress occurred during supination, which contrasts with the peak of soft tissue stress observed in pronation. When scrutinizing the tissue and splint stress through a 3D finite element model of Colles fracture during pronation, median rotation and supination, notable findings emerged. Consequently, it is deduced that anatomical splint fixation during median rotation proves efficacious in averting the localized compression of soft tissue.

Acknowledgements

Not applicable.

Funding

The present study was supported by the Scientific Research Project of Traditional Chinese Medicine Bureau of Guangdong Province (grant no. 20201170).

Availability of data and materials

The data generated in the present study are available from the corresponding author upon reasonable request.

Authors' contributions

Conception and design was by FH. RT and MWW provided administrative support. Provision of study materials or patients was by RT, LCH, MW and ZW. Collection and assembly of data was by SDS and JWH. Data analysis and interpretation was by YWL. FH and YWL confirm the authenticity of all the raw data. All authors participated in writing the manuscript. All authors read and approved the final manuscript.

Ethics approval and consent to participate

The present study was approved by the Ethics Committee of The Third Affiliated Hospital of Guangzhou University of Chinese Medicine and oral informed consent was obtained from the patient.

Patient consent for publication

Not applicable.

Competing interests

The authors declare that they have no competing interests.

References

1. Blakeney WG: Stabilization and treatment of Colles' fractures in elderly patients. Clin Interv Aging 5: 337-344, 2010.
2. Uppal G, Thakur A, Chauhan A and Bala S: Magnesium based implants for functional bone tissue regeneration-A review. J Magn Alloys 10: 356-386, 2022.
3. Mellstrand-Navarro C, Pettersson HJ, Tornqvist H, Tornqvist H and Ponzer S: The operative treatment of fractures of the distal radius is increasing: Results from a nationwide Swedish study. Bone Joint J 96-B: 963-969, 2014.
4. Hua Z, Wang JW, Lu ZF, Ma JW and Yin H: The biomechanical analysis of three-dimensional distal radius fracture model with different fixed splints. Technol Health Care 26: 329-341, 2018.
5. Taylor M and Prendergast PJ: Four decades of finite element analysis of orthopaedic devices: Where are we now and what are the opportunities? J Biomech 48: 767-778, 2015.
6. Yu XF: The Analysis of the curative effect of different surgical methods on distal radius fracture and biomechanical analysis of associated three-dimensional finite element analysis model. Shijiazhuang: Hebei Medical University, 2021. Available from: https://d.wanfangdata.com.cn/thesis/D02511085.
7. Clough RW: The Finite Element Method in Plane Stress Analysis. 1960. Available from: https://www.mendeley.com/catalogue/3dce7055-cde9-3d07-b2a8-712b203dd6a2/.
8. Rybicki EF, Simonen FA and Weis EB Jr: On the mathematical analysis of stress in the human femur. J Biomech 5: 203-215, 1972.
9. Brekelmans WA, Poort HW and Slooff TJ: A new method to analyse the mechanical behaviour of skeletal parts. Acta Orthop Scand 43: 301-317, 1972.
10. Xiong H and Nie W: Accurate simulation of stress state in bone joint and related soft tissue injury by three-dimensional finite element analysis. Chi J Tissue Eng Res 26: 5875-5880, 2022.
11. Yang X, Li Y L and Liu DJ: Progress in the application of three-dimensional finite element analysis in anterior cruciate ligament reconstruction. Chi J Sports Med 39: 742-745, 2020.
12. Marongiu G, Leinardi L, Congia S, Frigau L, Mola F and Capone A: Reliability and reproducibility of the new AO/OTA 2018 classification system for proximal humeral fractures: A comparison of three different classification systems. J Orthop Traumatol 21: 4, 2020.
13. Fishman EK: CT scanning and data post-processing with 3D and 4D reconstruction: Are we there yet?. Diagn Interv Imaging 101: 691-692, 2020.
14. White NJ and Rollick NC: Injuries of the scapholunate interosseous ligament: An update. J Am Acad Orthop Surg 23: 691-703, 2015.

15. Wang HJ: Atlas of Human Anatomy. Beijing: People's Medical Publishing House Co., Ltd., 2005:411. Available from: https://book.douban.com/subject/1448343/.
16. Xie RG, Tang JB and Tang TS: Morphological and arthroscopical observation of the triangular fibrocartilage complex of wrist. Chi J Joint Surg (Electronic Edition) 1: 41-45, 2011.
17. Çelik A, Kovacı H, Saka G and Kaymaz İ: Numerical investigation of mechanical effects caused by various fixation positions on a new radius intramedullary nail. Comput Methods Biomech Biomed Engin 18: 316-324, 2015.
18. Mouzakis DE, Rachiotis G, Zaoutsos S, Eleftheriou A and Malizos KN: Finite element simulation of the mechanical impact of computer work on the carpal tunnel syndrome. J Biomech 47: 2989-2994, 2014.
19. Wei B, Xu ZC and Chang S: Biomechanical properties of the lumbar pedicle screws by finite element analysis. Chin J Tissue Eng Res 22: 3091-3096, 2018.
20. Xia CJ, Yuan ZF and Fang N: Biomechanical characteristics of the distal radius fracture based on three-dimensional finite element model of ulna and radius. Chi J Tissue Eng Res 24: 893-897, 2020.
21. Matsuura Y, Kuniyoshi K, Suzuki T, Ogawa Y, Sukegawa K, Rokkaku T and Takahashi K: Accuracy of specimen-specific nonlinear finite element analysis for evaluation of distal radius strength in cadaver material. J Orthop Sci 19: 1012-1018, 2014.
22. Qin B, Huang YH and Ouyang Y: Finite element analysis in scaphoid bone under action of axial stress. J Army Med University 32: 1213-1315, 2010.
23. Li X: Splint binding force of small splint for distal radius fracture on the elders: A clinical and experimental quantitative research. Guangzhou: Guangzhou University of Chinese Medicine, 2011. Available from: https://cdmd.cnki.com.cn/Article/CDMD-10572-1011132640.htm.
24. Wu ZP, Gao WY and Wu LJ: Progress of finite element analysis on biomechanics of the wrist joint. Int J Orthop 29: 307-309, 2008.
25. Zhou XN: Establishment of three-dimensional finite element model of wrist joint and biomechanical analysis of distal radius fracture. Beijing: Beijing University of Chinese Medicine, 2014. Available from: https://cdmd.cnki.com.cn/Article/CDMD-10026-1014242530.htm.
26. Shapiro JA, Feinstein SD, Jewell E, Taylor RR, Weinhold P and Draeger RW: A biomechanical comparison of modified radioscapholunate fusion constructs for radiocarpal arthritis. J Hand Surg Am 45: 983.e1-e7, 2020.
27. Wang D, Li Y, Yin H, Li J, Qu J, Jiang M and Tian J: Three-dimensional finite element analysis of optimal distribution model of vertebroplasty. Ann Palliat Med 9: 1062-1072, 2020.
28. Grafstein E, Stenstrom R, Christenson J, Innes G, MacCormack R, Jackson C, Stothers K and Goetz T: A prospective randomized controlled trial comparing circumferential casting and splinting in displaced Colles fractures. CJEM 12: 192-200, 2010.
29. Li DL and Shi JM: Efficacy analysis of different treatment on distal radius comminuted fracture in elderly patients. Chi J Trad Med Traumatol Orthop: 41-43, 2012.
30. Huang AY, Li GQ and Cao LB: Treatment of 270 cases of colles fracture with Li's Manual reduction and willow splint fixation. J Ext Ther Trad Chi Med: 64-66, 2022.
31. Salmon P: Loss of chaotic trabecular structure in OPG-deficient juvenile Paget's disease patients indicates a chaogenic role for OPG in nonlinear pattern formation of trabecular bone. J Bone Miner Res 19: 695-702, 2004.
32. Wear KA: Mechanisms of interaction of ultrasound with cancellous bone: A review. IEEE Trans Ultrason Ferroelectr Freq Control 67: 454-482, 2020.
33. Steiner JA, Ferguson SJ and van Lenthe GH: Computational analysis of primary implant stability in trabecular bone. J Biomech 48: 807-815, 2015.
34. Knothe Tate ML, Tami AE, Netrebko P, Milz S and Docheva D: Multiscale computational and experimental approaches to elucidate bone and ligament mechanobiology using the ulna-radius-interosseous membrane construct as a model system. Technol Health Care 20: 363-378, 2012.
35. Oliva F, Buharaja R, Iundusi R and Tarantino U: Leg fracture associated with synostosis of interosseous membrane during running in a soccer player. Transl Med UniSa 17: 1-5, 2018.
36. He J, Ma X, Hu Y, Wang S, Cao H, Li N, Wang G, Guo L and Zhao B: Investigation of the characteristics and mechanism of interosseous membrane injuries in typical maisonneuve fracture. Orthop Surg 15: 777-784, 2023.
37. Adams JE, Culp RW and Osterman AL: Interosseous membrane reconstruction for the Essex-Lopresti injury. J Hand Surg Am 35: 129-136, 2010.
38. Thangavel M and Elsen Selvam R: Review of physical, mechanical, and biological characteristics of 3D-Printed bioceramic scaffolds for bone tissue engineering applications. ACS Biomater Sci Eng 8: 5060-5093, 2022.